Virtual process for evaluating the influence of real combined module variations on the overall performance of an aircraft engine

Jan Goeing[1,*], Hendrik Seehausen[2], Lennart Stania[2], Nicolas Nuebel[3], Julian Salomon[4], Panagiotis Ignatidis[5], Friedrich Dinkelacker[5], Michael Beer[4], Berend Denkena[3], Joerg R. Seume[2], Jens Friedrichs[1]

[1]Institute of Jet Propulsion and Turbomachinery, Technische Universitaet Braunschweig, Hermann- Blenk- Str. 37, 38108 Braunschweig, Germany
[2]Institute of Turbomachinery and Fluid Dynamics, Leibniz Universität Hannover, An der Universität 1, 30823 Garbsen, Germany
[3]Institute of Production Engineering and Machine Tools, Leibniz Universität Hannover, An der Universität 2, 30823 Garbsen, Germany
[4]Institute of Risk and Reliability, Leibniz Universität Hannover, Callinstr. 34, 30167 Hannover, Germany
[5]Institute of Technical Combustion, Leibniz Universität Hannover, An der Universität 1, 30823 Garbsen, Germany

Abstract

The effects of real combined variances in components and modules of aero engines, due to production tolerances or deterioration, on the performance of an aircraft engine are analysed in a knowledge-based process. For this purpose, an aero-thermodynamic virtual evaluation process that combines physical and probabilistic models to determine the sensitivities in the local module aerodynamics and the global overall performance is developed. Therefore, an automatic process that digitises, parameterises, reconstructs and analyses the geometry automatically using the example of a real turbofan high-pressure turbine blade is developed. The influence on the local aero-dynamics of the reconstructed blade is investigated via a computational fluid dynamics (CFD) simulations. The results of the high-pressure turbine (HPT) CFD as well as of a Gas-Path-Analysis for further modules, such as the compressors and the low-pressure turbine, are transferred into a simulation of the performance of the whole aircraft engine to evaluate the overall performance. All results are used to train, validate and test several deep learning architectures. These metamodels are utilised for a global sensitivity analysis that is able to evaluate the sensitivities and interactions. On the one hand, the results show that the aerodynamics (especially the efficiency η_{HPT} and capacity $\dot{m}_{HPT}$) are particularly driven by the variation of the stagger angle. On the other hand, η_{HPT} is significantly related to exhaust gas temperature (Tt5), while specific fuel consumption (SFC) and mass flow $\dot{m}_{HPT}$ are related to HPC exit temperature (Tt3). However, it can be seen that the high-pressure compressor has the most significant impact on the overall performance. This novel knowledge-based approach can accurately determine the impact of component variances on overall performance and complement experience-based approaches.

Introduction

Novel aircraft engines, such as the ultra high-bypass aircraft engines, will play a crucial role in the future development and increased efficiency of modern aircraft Merkl (2016). Since the performance and, above all, the economy of an aircraft are directly and inextricably linked to the

performance of the aircraft engine, constant efforts are being made to increase both the thrust generation and the fuel efficiency of engines. These continuing demands for more power and less fuel consumption ultimately lead to new and modern engine architectures that work even closer to the aerodynamic, thermal, and structural limits of the various components of the whole jet engine von der Bank et al. (2014).

However, the resulting design optimisations and modifications (e.g., 3D optimised blades) lead to more complex parts and functional integration within a part or assembly and thus also to an increasing sensitivity in geometric variations. Due to the high degree of interactions between the components and between individual parts within the components, geometry deviations that occur due to manufacturing and repair tolerances, as well as deterioration (e.g., erosion), can have a much greater impact on efficiency and performance than in previous generations of aircraft engines. Lavainne (2003) describes the geometry variations of compressor blades and names typical production scatter in the order of up to 1.5% in the chord length, 0.8% in the leading or trailing edge thickness, and 2.5% in stagger angle. Particularly in the case of modern aircraft engines, where experience and data are not available, knowledge-based approaches that investigate the influence of geometric variances on the overall system are essential.

Therefore, in Reitz et al. (2018) a virtual process for geometric evaluation of compressor blades was developed to determine the influence of geometry variations. Using measured compressor blades, high sensitivites of the loss coefficient and efficiency to aerodynamic blade parameters such as camber and stagger angle were identified.

Furthermore, Bammert and Sandstede (1976) already investigated the effects of manufacturing tolerances on the performance of turbines. For example, the enthalpy decreased by 15%, mass flow increased by 15%, and efficiency of the axial turbine fell by 1.4% when the blade thickness was reduced for the first two stages of a four-stage axial turbine. A thickening of the last two stages of the same turbine, on the other hand, causes an increase in the enthalpy gradient by 6% and a drop in the mass flow by 6%. The efficiency drops disproportionately by 3%. In Schwerdt et al. (2017), investigations were carried out on worn and factory-new first-stage turbine rotors. For this purpose, both blades were digitised using a 3D laser scanner, built up as a numerical model and numerical simulations were carried out. In the evaluation, differences were detected in the pressure and temperature field on the blade surface of the examined blades.

Based on the production and deterioration as well as repair influences, there are no exactly identical blades; each blade has its own individual parameter combinations within the permissible production tolerances. Consequently, each blade has individual aerodynamic properties. Numerical analysis of each individual blade is not practical, rather, probabilistic studies are used for simple analysis of the individual parameters. In Scharfenstein et al. (2013), 500 blades were digitally measured and evaluated. For this purpose, the three-dimensional geometry was reduced to two-dimensional sections and completely described by means of 14 blade parameters (Heinze et al., 2014). With the help of these determined parameters, it was possible to set the limits for the random generation of the samples, which were used in a Monte Carlo simulation. A sample of 50 blades showed that there is a strong dependence of the reduced mass flow and reaction degree on the stagger angle, as well as a strong dependence of the efficiency to the trailing edge thickness. A similar probabilistic approach was used by Ernst et al. (2016) for analysing a data set containing of 20 measured low-pressure turbine (LPT) blades that showed significant geometric variations due to operation. The probabilistic simulations with 100 samples were performed for several operating points that showed a strong dependency on the chosen operating point. The polynomial-based sensitivity analysis identified the stagger angle and the trailing edge thickness as the most important parameters for the change in aerodynamic efficiency.

In Gilge et al. (2019), real surfaces of worn compressor blades of a conventional high-bypass turbofan were measured and evaluated. The variations can be seen both in the roughness height (quantified by the roughness parameters) and qualitatively in the shape of the roughness structures. These structures are oriented at an angle of 45° to 90° perpendicular to the flow direction and are caused by oil and flow particles.

In Seehausen et al. (2020), the obtained roughness information was transferred to a CFD model of the V2500-A1 high-pressure compressor and the effect of complex surface structures on the overall compressor performance was evaluated. The simulations with stage roughness variations show that the first stage has the greatest impact on compressor performance. Furthermore, the surface roughness influences the narrowing and displacement of the compressor maps to a high degree, thereby decreasing the pressure ratio much more significantly than the capacity and efficiency in all speed curves considered. In general, these studies show that geometry variations and surface roughness have a significant influence on the integral pressure ratios π, mass flows $\dot{m}$, and efficiencies η, which directly affects the overall performance of the whole aircraft engine and can be investigated by gas path analysis (Spieler et al., 2008; Volponi, 2014).

In Goeing et al. (2020a), the findings of the roughness study already discussed were transferred into a whole aircraft engine performance simulation program and their effect on the overall performance was analysed at various steady-state operating points and transient manoeuvres. It was shown that the exhaust gas temperature is increased by more than 20% at steady-state operating points and transient temperature loads by up to 30%. Furthermore, combined deterioration of high-pressure compressor (HPC) and HPT was investigated in Goeing et al. (2020b). The characteristic effects of the investigated deterioration on performance can be summarised as follows:

1. SFC and Tt5 can be used to determine the degree of deterioration.
2. Temperature downstream the combustor (Tt4) and the rotational speeds in combination can be used to identify the components affected by the deterioration.
3. The distance to the stability limit in the HPC and the deviation between the transient and steady-state operating lines differ significantly for HPT and HPC deterioration.
4. Both HPC and HPT degradation have significant influences on the global engine behaviour, but HPC degradation has a significantly stronger effect on the stability of the engine.

The methods described above usually focus on a single module or the module interactions, but do not connect all process steps (see Figure 1). To meet the requirements of the Collaborative Research Centre (CRC) 871 'Product Regeneration', which captures both, the system complexity and the degradation of system components in order to provide the fundamentals for an efficient regeneration of complex capital goods such as high-bypass aircraft engines, a communication structure between the process steps is developed. The communication structure with the virtual twin of the aircraft engine, which allows to assess the performance of individual blades and to obtain module-based sensitivities, enables interaction with a virtual twin of the regeneration in order to choose regeneration paths.

In this work, the developed process is demonstrated using the first stage of the HPT blade of the V2500 turbofan engine as an example in a high Technology Readiness Level of 7. The V2500 turbofan with low-pressure compressor (LPC), intermediate-pressure compressor (IPC), HPC, HPT, LPT, and a common thrust nozzle, from IAE (International Aero Engines) typically powers the Airbus A320-100 representing medium-range aircraft. The paper discusses first how the blades used are digitised, parameterised and reconstructed automatically for an automated meshing process. Subsequently, the CFD set-up and the performance simulation are outlined, and both, the sensitivity analyses and the metamodels employed are presented. A DoE is carried out to quantify the global sensitivities of geometry variations and aero-thermodynamics. Finally, the virtual process is run on the best and worst HPT blades to illustrate the influence of isolated and combined module variances on the performance. This combines the different methods for evaluating local aerodynamics and global performance, providing a knowledge-based process that examines the causalities between component variations and performance changes from the bottom up.

Methodology for the evaluation of the virtual twin of the aeroengine

In this chapter, the single steps of the virtual process for a component evaluation are discussed (see Figure 1). The virtual analysis is carried out on the example of the first HPT rotor stage blade of the V2500-A1. Based on
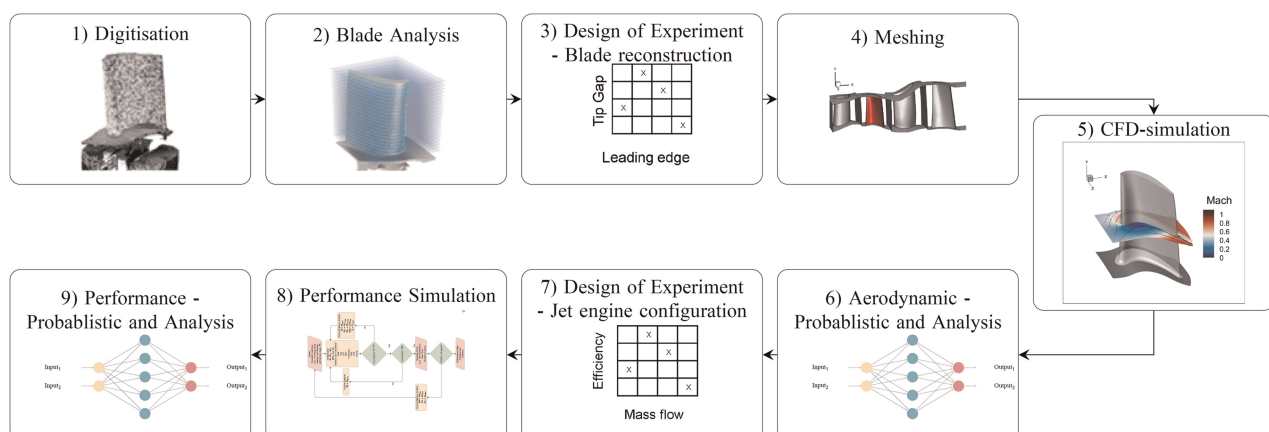

Figure 1. Virtual performance evaluation process of the system demonstrator.
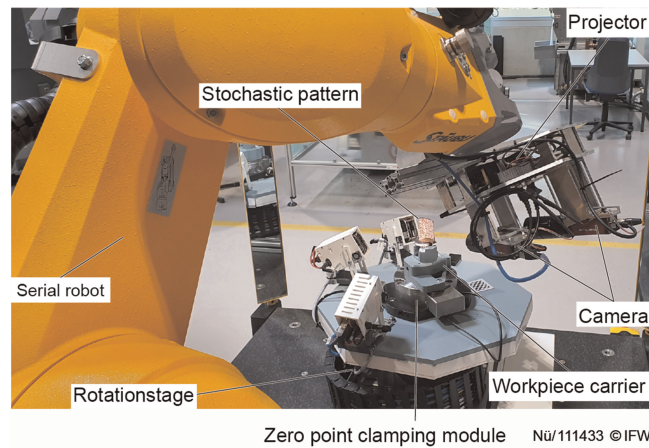
Figure 2. Measurement system scanning a blade.

the IFAS research aircraft engine, performance data of the V2500-A1, information, and geometries of the HPT, which are necessary for a CFD set-up, are available. In order to develop the real repair process in CRC 871 (Aschenbruck et al., 2014), a large number of HPT-blades were required. This high number could not be provided by the V2500-A1, so the repair process was developed on scraped HPT-blades of the V2500-A5.

Digitisation of HPT blades

A fringe projection system is used (Betker et al., 2020) for the digitisation of the blade geometry. In order to automate the process and reduce systematic errors, the projector and camera of the measuring system are positioned with a serial robot (see Figure 2). The projector projects an alternating stripe pattern on the scraped and heavily deteriorated blades to measure the geometry from root to tip. The camera captures the deflection of the stripes. A measuring computer calculates the distance to the camera from these images and creates a point cloud from it. With a high dynamic range measurement, blades with different optical surface properties can be measured.

The blade is clamped using a workpiece carrier and a zero point clamping module, that is mounted on a rotation stage. On this stage, three projectors are mounted and project a stochastic pattern on the blade. This pattern, overlapping measurements, and the special geometry of the workpiece carrier are then used to merge the point clouds of the 13 single measurements to a combined point cloud.

The coordinate system of the measurement system is calibrated once with a normal. Because of the low absolute accuracy, as well as the assembly tolerances of the workpiece carrier, the position and orientation of the measured blade varies in the fixed coordinate system. An iterative closest point algorithm aligns the worn blade to a reference blade to determine the parameters of each blade on the same positions. After the alignment, blade slices of 1.2 mm around the planes that are used in the next steps are extracted and parameterisation (±600 μm) are extracted and converted into a 3D-model with surfaces. Additionally, a convex hull is used which allows the robust closing of holes from heavy damage and cooling air holes.

The alignment is performed by an Iterative Closest Point Algorithm. The alignment is carried out globally, since individual geometry parameters are not sufficient due to the geometry variations. Due to the strong wear in the blade tip, the alignment is only used in the range from the foundation to 5 mm below the blade tip. The iteration is converged if the change is less than 3 micrometers or 30 iterations are exceeded (Nübel and Denkena, 2022).

After the marcrosopic geometric properties of the investigated blades, the small-scale surface structures are optically measured with a con-focal laser scanning microscope (Keyence VK-X200). In the process, the measurement of surface roughness is performed at five positions on the suction side and at four positions on the pressure side at mid-span with a 20× magnification lens. For CFD simulations an equivalent sand-grain roughness k_s is required to analyse surface roughness and compare different rough surfaces. In Nikuradse (1933) and Schlichting (1936) the equivalent sand-grain roughness was introduced, which describes the aerodynamic resistance of the surface roughness. In Bons (2010) a detailed overview of established correlations for converting a technical roughness to an equivalent sand-grain roughness is described. To assess the complexity of a three dimensional roughness topology, Hohenstein et al. (2013) and Gilge et al. (2019) propose using the shape and density parameter

Λ_s of Sigal and Danberg (1990). Therefore, the approach of Bons (2005):

$$\log\left(\frac{k_s}{k}\right) = -0,43\log(\Lambda_s) + 0,82 \tag{1}$$

with the roughness parameter k described by the surface parameter S_a as proposed by Gilge et al. (2019) is used in this process. Here, the equivalent sand-grain roughness is averaged separately along the suction and the pressure side.

Parameterisation

The digitised blade is analysed in 20 different blade sections at constant radial positions based on the slices from the digitisation. Each blade section is parameterised by algorithms based on Heinze et al. (2014) and Ernst et al. (2016) and exemplified in Figure 3. The camber is approximated by the Delaunay triangulation (Aurenhammer, 1991), where the middle points of enveloping circles around the Delaunay triangles correspond to the camber line. This approach fails near regions with high curvature, e.g. leading- or trailing -edge. Therefore, different filters, based on the curvature of the camber, are applied in regions near the trailing- and the leading-edge in order to remove outliers. The leading-edge camber is approximated by a second order function attaching to the estimated camber based on the Delaunay triangulation and the trailing-edge by a first-order function, resulting in crossings with the blade´s macroscopic geometry. These crossings are the leading-edge and trailing-edge stagnation points which are used for rotating the blade around the origin and shifting the profile that the leading-edge stagnation point is placed at the coordinate system´s origin and the trailing-edge is horizontally aligned with the origin. This simplifies further calculations. The leading-edge radius r_{LE} is approximated by fitting a circle within the given blade geometry using a least-square method solved by a Levenberg-Marquardt algorithm (Moré, 1978). This algorithm is used also for fitting an ellipse at the trailing-edge giving the parameter a_{TE} along the camber line axis and b_{TE} orthogonal to the camber. Furthermore, the curvature of the camber line has to be within certain defined tolerances. Stagger angle γ and chord length l are calculated by trigonometric functions. The geometric parameters considered in this work are shown in Table 1 including their absolute ranges and 95% confidence intervals. The absolute ranges are derived of the min-max value of each geometric parameter within the 36 digitised blades. The measurement accuracy of the digitisation and parameterisation is determined by measuring two blades in five different fixtures. The point clouds are aligned and the parameters extracted. The maximum deviation for each parameter is used as approximation of the measurement accuracy. Additionally, the range of
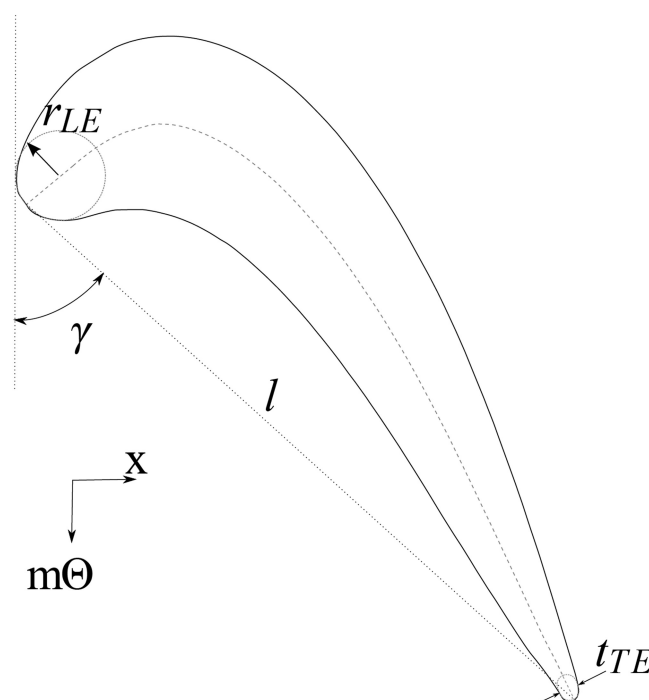

Figure 3. Blade section of deteriorated blade at mid-span.

Table 1. Digitised blade parameters as in the example in Figure 4.

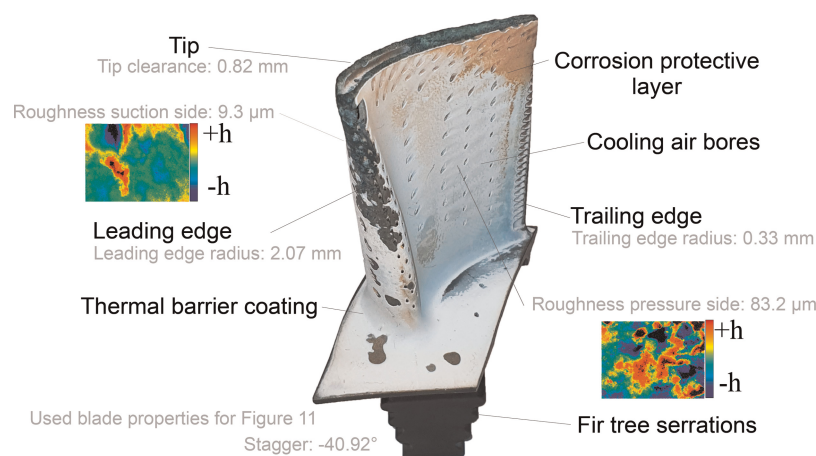|	Tip gap in mm	Leading edge radius in mm	Chord length in mm	Trailing-edge thickness in mm	Stagger angle in °	Roughness suction side k_s in μm	Roughness pressure side k_s in μm
symbol	R	r_{LE}	l	t_{TE}	γ	R_{SS}	R_{PS}
Max	1.64	2.32	32.73	1.1	−40.34	32.07	118.6
Min	0.59	1.96	32.01	0.25	−45.15	4.19	11.4
95% CI	±0.05	±0.05	±0.15	±0.05	±0.30	±1.46%	±1.46%

Figure 4. Heavily deteriorated HPT blade used in this project.

surface roughness applied to the CFD simulations is presented with a relative error of the optical measurements based on a confidence level of 95% (see Gilge et al. (2019)).

Reconstruction of HPT blade and sample generation

The blade reconstruction is performed using an original CAD blade geometry and altered based on the difference between reference and measured blades. This difference is applied for all blade sections along the span. In this work, the reference blade is defined as the least deteriorated one. Changing the geometry of the leading- and trailing edge requires smoothing between the new circles (for leading-edge) or ellipses (for trailing-edge) and the rest of the profile geometry for obtaining a continuous surface. Otherwise, the algorithm used is based on Ernst et al. (2016).

The ranges of the parameters are shown in Table 1 and a total of 250 blades with different geometries is reconstructed, each representing a combination of different geometry parameters and surface roughness. In order to carry out the numerical experiment effectively, a uniform Latin-hypercube sampling (McKay et al., 2000) is used. The tip gap variations are included during the meshing process. The roughness is implemented in the CFD setup on both, the suction and the pressure side. The digitised blades of the first rotor stage belong to a V2500-A5, while only original blade geometries of all rows of the V2500-A1 are available for usage in the computational models. To overcome this issue, the geometric variations are normalised with the blade height, assuming that both variants of the V2500 show geometrically similar wear.

CFD simulations of HPT with deteriorated first rotor

Based on the reconstructed blades, numerical set-ups are developed and simulated in a fully automated process. The CFD simulations are necessary to connect the effects of local deterioration, here first rotor blade, with the module performance. First, the meshes of the 2-stage HPT are constructed using *Numeca Autogrid*. The

meshing parameters are set constant for all reconstructions to ensure mesh independence of the numerical solution. According to the DoE, the different tip gaps are included in the meshing. A total of 211 HPT simulations with a deteriorated first rotor blade are successfully meshed. For 39 combinations of geometric parameters, the meshing fails due to negative cell volumes or connectivity problems across the rows. In Figure 5 a mesh of an HPT is illustrated with the first blade highlighted in red. The original HPT geometry was already used in Goeing et al. (2020b) for evaluating combined compressor and turbine deterioration. Secondly, the simulations are performed using the non-commercial flow solver *TRACE* version 9.1 of the German Aerospace Center (DLR) (Nuernberger, 2004; Franke et al., 2005; Kugeler et al., 2008). The three-dimensional Favre-averaged Navier-Stokes equations are solved by a finite-volume method with structured multi-block meshes. Roe's second-order upwind scheme is used for the discretisation of the convective fluxes, while the diffusive fluxes are solved by a second order central difference scheme. In an automated pre-processing, the boundary conditions of the aerodynamic design point at take-off with a rotational speed of 13,972 rpm prescribed by the performance simulation are transferred to the CFD set-up. Next to the boundary conditions, the equivalent sand-grain roughness k_s is specified at suction and pressure side of the first blade row. At the inlet, a total pressure of approximately 2,823 kPa and a total temperature of approximately 1,735 K is used. Additionally, a turbulence intensity of 4% and a turbulent length scale of 0.00208 m is set, which are typical for turbomachinery flows. At the outlet, a static pressure of 491.6 kPa is specified. Subsequently, periodic steady-state simulations with one pitch are conducted using the $k - \omega$ turbulence model of Wilcox (1988), assuming that the analysed blade represents the entire row. For the blade to vane interfaces mixing planes are used and the stagnation point anomaly fix by Kato and Launder (1993) is applied. The sidewalls are modelled through a wall function. In general, a non-dimensional distance of the first cell from the wall of $y^+ < 1$ is obtained at the blade's surfaces, which allows resolving the viscous sublayer using the Low-Reynolds approach. Nevertheless, the first rotor blade is modelled by the wall function due to the increased wall shear stress caused by surface roughness. The logarithmic profile is described by:

$$\frac{U}{u_\tau} = u^+ = \frac{1}{\kappa}\ln\left(y^+\right) + C^+ \text{ with } u_\tau = \sqrt{\frac{\tau_w}{\rho}} \tag{2}$$

as friction velocity u_τ. As a result of rough surfaces, the value C^+ of the logarithmic profile is expressed as a function of k_s, which results in:

$$C^+ \rightarrow \frac{1}{\kappa}\ln\left(\frac{1}{k_s^+}\right) + 8.4 \tag{3}$$

according to Wilcox (1988). A post-processing is applied to calculate the pressure ratio π and the polytropic efficiency η_{poly} of each generated sample. The polytropic efficiency η_{poly} is calculated from the total pressure ratio π and the total temperature ratio τ as follows:

$$\pi = \frac{p_{\text{t,out}}}{p_{\text{t,in}}}, \quad \tau = \frac{T_{\text{t,out}}}{T_{\text{t,in}}}, \quad \eta_{\text{poly}} = \frac{\kappa - 1}{\kappa}\frac{\log\left(\pi\right)}{\log\left(\tau\right)}. \tag{4}$$

　　Although an accurate initial flow solution is used, a CFD simulation of a mesh with approximately 8 M cells requires about 84 CPUh for a converged solution. A mass flow difference between inlet and outlet, a change in efficiency, and a change in pressure ratio of less than 0.1% satisfy the stopping criterion.
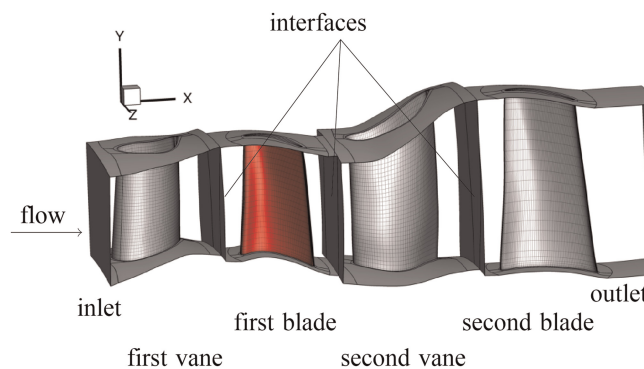

Figure 5. HPT simulation setup with studied first rotor blade highlighted in red.

For the validation the original CAD blade geometry with a hydraulically smooth surface is used. The CFD simulations predict a polytropic efficiency of 88.68%, a pressure ratio of 5.2, and a massflow of 47.28 kg/s, while performance simulation gives 88.80%, 5.1 and 48.02 kg/s for same boundary conditions. With the same setup a mesh convergence study is conducted, resulting in a GCI of 0.136% for the mass flow, 2.59% for the polytropic efficiency, and 0.005% for the pressure ratio.

Performance simulation of the overall aircraft engine

In order to evaluate the influence of isolated and combined module variances on the whole turbofan engine a performance model of the V2500-A1 aircraft engine is developed to analyse the on- and off-design performance. The model is part of a model-based non-linear gas path analysis (NLGPA) to calibrate the performance model to real aircraft engines (here a factory-new and deteriorated V2500-A1 turbofan engine (see Table 2)).

This analysis investigates the ranges in which the miscellaneous compressors and turbines wear out in addition to the HPT. In conjunction with the CFD simulations of the HPT, the NLGPA and, thus, the virtual process allow a combination of the overall aircraft engine performance with the local effect of deterioration. This analysis is presented by the schematic flow chart illustrated in Figure 6 and is implemented in Matlab (Kurzke and Halliwell, 2018; Salomon et al., 2021).

The off–design calculation procedure consists of an iterative simulation process which requires various input data, such as environmental conditions. Moreover, further aircraft engine-specific boundary conditions are required, being crucial for the thermodynamic cycle at a reference point, also referred to as the engine's on–design operating point. This point represents the basic framework of the jet engine and defines the interaction between the miscellaneous turbomachines, secondary air system, geometry (e.g. nozzle area), and number of revolutions in order to fulfil the thermodynamic cycle. Further boundary condition, such as the steady-state performance maps of the compressors and turbines are required. Hereon, quantities related to the compressor and turbines are denoted with $(.)_C$ and $(.)_T$ sub-indexes, respectively. These characteristic diagrams describe the mass flow $\dot{m}$, pressure ratio π, and efficiency η of the turbomachines by different rotational speeds. Furthermore, auxiliary coordinates, the so-called GL–lines, are placed through the diagram, which are necessary for the iteration of the algorithm. The on-design performance values and the boundary conditions for the V2500-A1 jet engine are based on Goeing et al. (2020b), as well as on the data of the IFAS-research aircraft engine.

After the aircraft engine–specific boundary conditions have been imported and the operating point to be reached has been defined, the analysis starts the iterations. A distinction is made between the outer loop, in which the rotational speed N_2 is varied until the required aircraft engine thrust is reached, and the inner loop, in which a correct thermodynamic cycle, based on the input parameters, is matched through iterations. Matching in this context means iterating within the performance maps until: (1) the turbine power P_T output matches the compressor power P_C, as defined by the error function E_P in Equation 5; (2) the mass flow is maintained, as defined by the error function $E_{\dot{m}}$ in Equation 6; and (3) the nozzle pressure $p_{nozzle,t8}$ is equal to the downstream LPT pressure $p_{LPT,t8}$ (including friction), as defined by the error function E_N in Equation 7. The convergence limits are 1e-6.

$$E_P = P_T - P_C = \Delta h_{tT} \cdot \dot{m} - \Delta h_{tC} \cdot \dot{m} \qquad (5)$$

$$E_{\dot{m}} = \dot{m}_T - \dot{m}_C \qquad (6)$$

$$E_N = p_{nozzle,t8} - p_{LPT,t8} \qquad (7)$$

Table 2. Maximum thrust 109 kN.

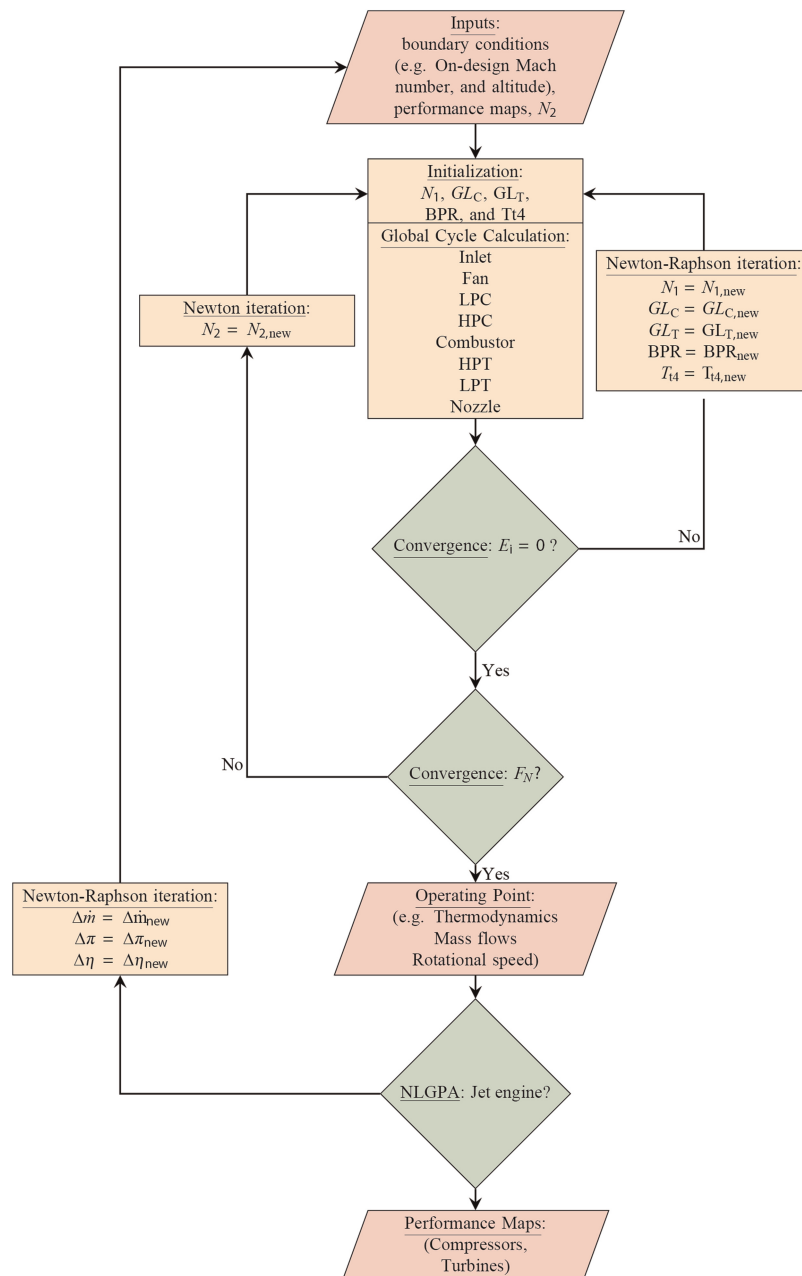| Value	SFC	Pt5	Tt3	Tt5	N1	N2
Unit	g/(kN·s)	kPa	K	K	rpm	Rpm
V2500-A1	10.23	142	850	806	4,981	13,972
IFAS - V2500 A1	10.56	138	835	850	4,959	13,757

Figure 6. Global off-design calculation procedure for high-bypass turbofans. Used for non-linear GPA and to train the artificial intelligence.

Based on the on–design input parameters, the initial values of all necessary parameters are provided for the first iteration. The iteration parameters for the inner loop at any rotational speed N_2 are the turbine entry temperature T_{TET}, bypass ratio (BPR), the rotational speed N_1, and the auxiliary coordinates GL_T and GL_C. Based on these, the operating point (constant thrust) of each individual aircraft engine is defined and a global cycle process calculation can be carried out. The next step is to validate whether Equations 5–7, are fulfilled and the error functions approaches zero. If this is not the case, then the iteration parameters are varied using the Newton–Raphson method until an operating point is found. The iteration parameter are varied throughout the ranges of all performance maps until a matching cycle according to Equations 5–7 is found. The next step is to check if this correct cycle also achieves the required thrust. If not, the rotational speed N_2 is varied using the Newton–Raphson method. Here the convergence limit is 1e-5.

The global aircraft engine matching process is described with these iterations and is used in the DoE to physically calculate the relationship between state of jet engine and performance output. The state of the engine is described by the variation of the maps through the scaling factors (Δ) of π, $\dot{m}$ and η.

In order to estimate the scaling factors for the LPC, IPC and HPC, as well as for the LPT, the performance model is calibrated to a factory-new and to the worn aircraft engine. The calibration is done via non-linear GPA, in which the performance map is iterated by scaling factors Δ via Newton-Raphson method until the performance model has the same performance output as the investigated aircraft engine. Here, the convergence limits are 2e-2 is assumed to be sufficient.

Sensitivity analysis

A fundamental knowledge of the effects of variations in the input variables of a model on the output variables is of paramount importance in a variety of engineering domains. Sensitivity analysis examines precisely these relationships. Saltelli et al. (2004) provide the following definition of sensitivity analysis: 'The study of how uncertainty in the output of a model (numerical or otherwise) can be apportioned to different sources of uncertainty in the model input'. Therefore, an effective and wide-ranged group of sophisticated sensitivity instruments are variance-based methods (Saltelli et al., 2010). The Sobol indices (Sobol, 2001) are a widely utilised representative of this type of sensitivity analysis tools for model outputs. These indices not only allow to identify the direct effects of particular input factors on the variances of output variables, but also of all potential impacts due to interaction effects between the variances of the inputs on the outputs.

Sobol indices

In the following text a brief description of the Sobol indices according to (Sobol, 2001; Saltelli et al., 2010; Kucherenko et al., 2012) is provided. For more information and a detailed derivation, see, e.g., (Sobol, 2001; Saltelli et al., 2010).

Consider a model $Y = f(x_1, x_2, \ldots, x_n)$ defined in $\mathbb{R}^n$ with Y denoting the model's output, f the model function and x_i the i-th real-valued random input variable with a distribution function $p(x_i)$. Let the input vector $x = (x_1, x_2, \ldots, x_n)$ be divided into two subsets $y = (x_{i_1}, x_{i_2}, \ldots, x_{i_s})$ with $1 \leq s < n$ and its complement $z = (x_{i_1}, x_{i_2}, \ldots, x_{i_{n-s}})$, so that $Y = f(x) = f(y, z)$. Then the total variance of Y can be written as:

$$V = V_y[E_z(f(y, z))] + E_y[V_z(f(y, z))]. \tag{8}$$

Normalising and decomposing Equation 8 by V leads to the closed-order effect index S_y and the total-effect index S_y^T with respect to subset y

$$S_y = \frac{V_y[E_z(f(y, z))]}{V} \qquad S_y^T = \frac{E_z[V_y(f(y, z))]}{V}. \tag{9}$$

Under the assumption of independent input variables, both Equations in 9 are known as Sobol indices. For the case of y being not arbitrary but univariate, i.e. $v = \{x_i\}$, $|v| = 1$, S_y is known as a first-order Sobol index, representing the contribution of x_i alone on the total variance of the output. The total-effect Sobol index S_y^T measures first and higher order effects, i.e., the contribution of x_i to the variance of the output, incorporating all variances caused by x_i's interactions with any other input variable or variables. Since the analytical determination of the Sobol indices is not feasible in the context of this work, the Monte Carlo based estimators according to Saltelli et al. (2010) are utilised.

Kucherenko indices

Even though Sobol indices are an excellent tool for conducting comprehensive variance-based sensitivity analysis, their applicability is based on the constraining assumption of independent input variables. However, in practical applications, such as the interdependent performance of the miscellaneous modules inside of an aircraft engine, this assumption might be untrue. In Kucherenko et al. (2012) an approach is provided to generalise the Sobol indices that allows to perform comprehensive sensitivity analyses, taking into account dependencies among input variables.

The first-order effect Kucherenko index is formulated according to Equation 9 as:

$$S_y = \frac{1}{V} \left[\int_{R^s} p(y) dy \left[\int_{R^{n-s}} f(y, \bar{z}) p(y, \bar{z}|y) d\bar{z} \right]^2 - f_0^2 \right], \tag{10}$$

and equivalent, the total-effect Kucherenko index is given by:

$$S_y^T = \frac{1}{2V} \int_{R^{n+s}} [f(y, z) - f(\bar{y}, z)]^2 p(y, z) p(\bar{y}, z|z) dy d\bar{y} dz, \tag{11}$$

with $\bar{z}$ being the notation specifying a random vector generated from the conditional joint density function $p(y, \bar{z}|y)$, distinct from vector z, generated by the non-conditional density function $p(y, z)$. $p(y)$ denotes the marginal distribution function of y, $p(y, \bar{z}|y)$ is the conditional probability density function of $\bar{z}$ given y and $f_0 = E(Y)$.

Note that the sum of all first-order effect Sobol indices is equal to or smaller than one, and the sum of all total-effect Sobol indices is equal to or greater than one (Glen and Isaacs, 2012). However, in the presence of dependencies in the model inputs, this does not hold for the Kucherenko indices. More information and a detailed derivation of the Kucherenko indices are provided in Kucherenko et al. (2012).

In practice, the analytical determination of the Kucherenko indices is often not feasible. Therefore, the present Monte Carlo estimators for their indices in Kucherenko et al. (2012), that are utilised in this work. Both estimators require a conditional sampling.

Metamodeling

In sensitivity analysis for the vast majority of cases, a relatively large sample size is mandatory. In aerodynamic engineering, however, many of the models employed are highly complex and simulations are consequently computationally demanding. As a result, generating sufficient samples is often too expensive or even unfeasible. A common approach to address this challenge is to develop and utilise metamodels that replicate the functionality of the original model, while being less complex and consequently less computationally intensive (see Shahsavani and Grimvall (2011) and Ben Abdessalem and El-Hami (2014)). In the context of aerodynamic engineering in general, and aircraft engine diagnostics in particular, such metamodels are increasingly based on artificial intelligence and deep learning approaches (see for example Khan and Yairi (2018) and Fentaye et al. (2019)). With these, larger sample sizes can be generated with less computational effort and thus, common sensitivity analysis tools can be applied.

In this work, artificial neural networks are trained to guarantee a sufficient sample size for the respective sensitivity analysis. A schematic layout of such a network is shown in Figure 7. It basically consists of an input layer, one or more hidden layers and an output layer. The number of neurons per layer, as well as the number of hidden layers, depends on the particular original model and cannot be generalised. The number of input neurons, as well as the number of output neurons, typically follows the number of input and output variables of the model to be mapped. Each neuron of a layer is weighted connected to each neuron of the predecessor and successor layer. For a detailed description of neural networks in general and fitting function networks in
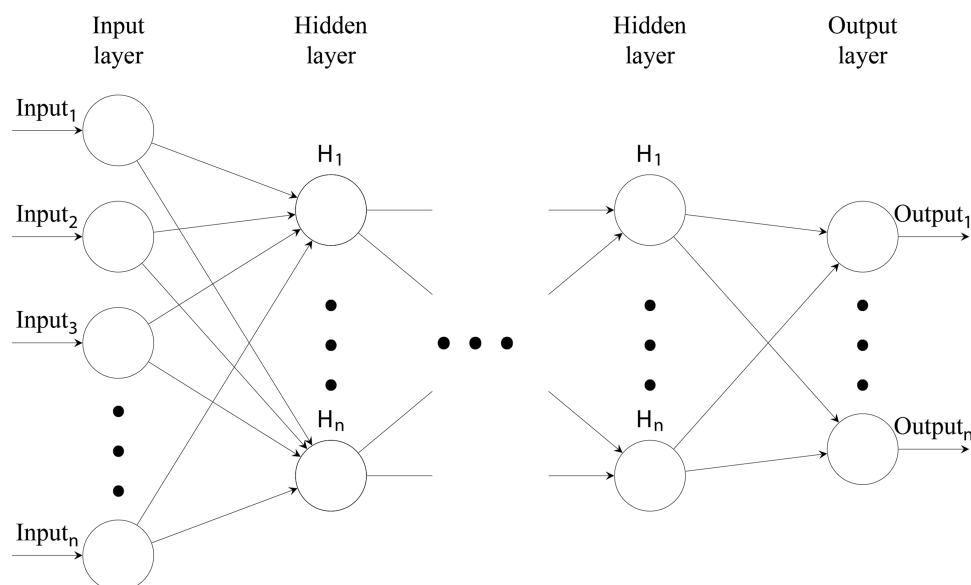

Figure 7. Architecture of a deep learning neural network.

particular, as well as their training and handling, see Rafiq et al. (2001) or Samarasinghe (2006). Note, that the utilization of an artificial neural network, such as employed in this work, represents only one potential approach among various approaches, such as, e.g., polynomial chaos expansion, to perform sensitivity analysis under the condition of a small data set. Here, the methods were exclusively chosen for the purpose to present proof of concept further methods will be investigated in subsequent work of the authors.

Results and discussion

The virtual process described in the methodology allows an instantaneous prediction of the effect of production scatter and of the deteriorated blades on the overall jet engine performance. Based on the physical model and metamodels the impact on aerodynamics and performance will be estimated.

HPT Sensitivities for single rotor deterioration

The performance sensitivity analysis of the overall aircraft engine requires significantly more than 211 performance samples of the HPT (see Figure 8). To expand the data, the described neural network as metamodel with three hidden layers, ten neurons per layer, eight input neurons, three output neurons, 15 epochs, and the Levenberg-Marquardt as back propagation algorithm is used. With these parameters a sufficient optimum was found, and for example, reducing the number of hidden layers results in a decrease in accuracy. Especially the epochs and neurons per layer showed an insensitivity for small changes in regards to prediction accuracy. For each neuron a sigmoid function is utilised as activation function. The final meta model reached a mean squared error of 1e-4 for all three outputs combined within a ten-times cross validation. Further improvement in accuracy would require more samples as well as further studies on different meta model approaches. The required extension of the geometric input is performed based on a Latin-hypercube sampling. Then, a variance-based sensitivity analysis is conducted on the input and output of the metamodel by means of Sobol indices (see Figure 9). This approach is validated by analysing the 211 original performance samples with the variance-based sensitivity approach according to Plischke (2010) and Plischke et al. (2013), so called EASI (Effective Algorithm for Computing Global Sensitivity Indices). This approach is purely based on existing data and does not require a specific input sampling. The sensitivity analysis is conducted on the three integral aerodynamic outputs in respect to the geometric inputs. First, a non-monotonic relationship is identified between mass flow and polytropic efficiency based on scatter plots. Classic correlation coefficients, e.g. Spearman's or Pearson's Rank correlation coefficient, are not sufficient in these cases. However, variance-based sensitivity studies are more suitable for detecting such non-monotonic relationships Saltelli et al. (2010). For the original CFD data the EASI indices of
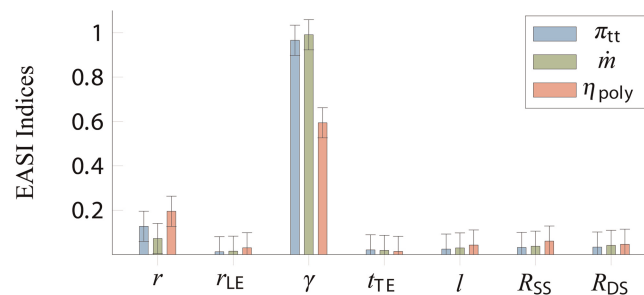

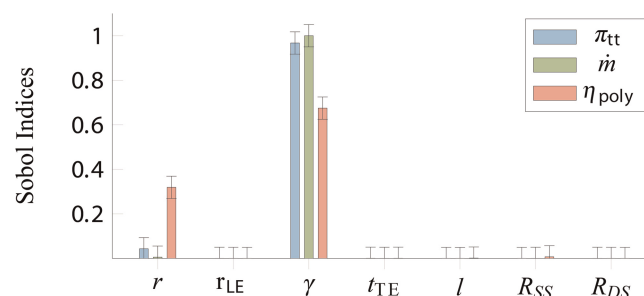Figure 8. EASI indices for CFD data.

Figure 9. Sobol indices after applying the HPT-metamodel.

first-order indicate a direct sensitivity between stagger angle γ on pressure ratio π and mass flow $\dot{m}$ approximately close to 1 (see Figure 8). This indicates negligible influence of the other geometric parameters for these output parameters. The EASI indices in Figure 8 show a sensitivity of around 0.1 for the influence of tip gap on pressure ratio and mass flow. However, due to the small sample size these results may include uncertainties and all other geometric parameters can be neglected. The polytropic efficiency has a sensitivity of 0.6 for γ and 0.2 for tip gap r. The influence of the tip gap is explained by the direct dependency of mass flow over the blade's surface resulting in higher pressure differences between pressure and suction side, and the leakage mass flow over the blades tip, which does not distribute to the turbines work conducted. The observation of the stagger angle agrees with the literature of Ernst et al. (2016) and Högner et al. (2016). The influence of the tip gap agrees with Yaras and Sjolander (1992).

The sample size is increased according to Saltelli et al. (2004) with $N = n \cdot (Number\ of\ Inputs + 2)$ with seven input parameters and $n = 2^{11}$ to $N = 18,432$ samples for the Sobol sensitivity analysis by means of Latin-hypercube sampling. For all inputs and outputs under consideration, a convergence study of the mean as well as of the 2nd to 4th central moment was conducted. All examined variables converge according to the sample size N employed. Solely the output π exhibits slight leaps in the 3rd and 4th central moment. However, these have no influence on the results obtained, see Figure 10. The relationships of the original data are confirmed on the metamodel output, which is shown in Figure 9. Leading-edge radius, trailing-edge thickness, chord and surface roughness on both blade sides are negligible for all output parameters. Mass flow is completely determined by the stagger angle. The polytropic efficiency has a Sobol index of 0.6 for the stagger angle and 0.35 for tip gap, which is increased for the tip gap by 0.15 in comparison with the approximation of the original data set. For the pressure ratio the sensitivity regarding the tip gap is decreased further and the stagger angle is held constant versus in the original data.

It is shown that the estimated variance-based sensitivity analysis of the original data is similar to the Sobol analysis with a metamodel based on the original data. However, for this study it is only possible to analyse the direct relationship between inputs and outputs, i.e., first-order indices. Higher-order effects, that can show the systems interactions of input variables and their combined influence on the output variables, require larger sample sizes. Subsequently, an analysis of total-order effects purely based on the metamodel can not be validated and is therefore not conducted within this study.

Performance analysis

In order to estimate the impact on the overall performance of the V2500-A1 aircraft engine, the ranges of the scaling factors of each turbomachine have to be estimated. These ranges are determined on the one hand by CFD of the HPT, and on the other hand by the NLGPA of a factory-new and operational stressed aircraft engine V2500 (see Figure 6 and Table 2). The resulting scaling factors are an identifier for the real range of degradation of the compressors and turbines in the turbofan. These parameters are validated by previous studies (Goeing et al., 2020a) and further literature (Maiwada et al., 2016; Cruz-Manzo et al., 2018) (see Table 3). Thus, the $\Delta \dot{m}$ and $\Delta \pi$ of the HPC have the most significant impacts (-8%), followed by $\Delta \eta$ of the HPT (-6%). Furthermore, the smallest impact was found for the LPT (-1% and -2%). Based on these scaling factors Δ, a uniform Latin-hypercube sampling is performed to simulate the performance of 200,000 different combinations of varying V2500-A1 turbofan engines at the same thrust level. Next, 70% of the results are used as a training set and 30% as a validation and testing set for the neural network. The mean square error of the metamodel is less than 1e-8.
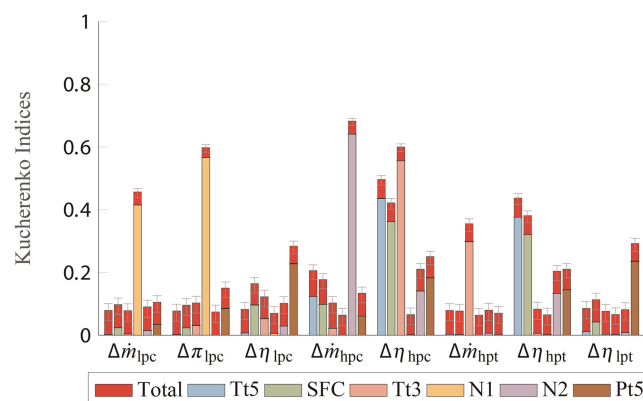

Figure 10. First and Total Kucherenko Indices of the scaling factors and overall performance output.

Table 3. Scaling factors based on CFD, NLGPA and Literature.

	LPC	IPC	HPC	HPT	LPT
$\Delta\dot{m}$	0.96	0.96	0.92	1.05	0.98
$\Delta\pi$	0.96	0.96	0.92	0.95	0.98
$\Delta\eta$	0.97	0.97	0.96	0.94	0.99

This metamodel is used with 1e6 random parameter configurations within the parameter space to evaluate the isolated and combined sensitivities. The input variables are interdependent, due to the power balance and mass conservation (see Equations 5 and 6), so a variance-based sensitivity analysis according to Kucherenko which is able to analyse such interdependent input variables is performed.

In Figure 10 the isolated (first) and isolated plus interacting (total) sensitivities of measurable variables are shown. Therefore, the first- order indices are represented with blue for Tt5, green (SFC), light red (Tt3), yellow (N1), purple (N2) and brown (Pt5) bars. The stacked red bars represent the total indices. Further on, the 95% confidence interval is shown as a black error bar for the first-order and a grey error bar for the total order. Scaling factors Δ (e.g. IPC or Combustor) with an influence of less than 0.05 are neglected for the sake of clarity.

As shown in Figure 10, most of the peaks are located at the HPC and HPT. In particular, the EGT (0.44/ 0.38) and the SFC (0.36/0.32) are responded to the efficiency of the HPC/HPT. It is noticeable that the temperature Tt3 reacts on the efficiency of the HPC (0.56), as well as the mass flow of HPT (0.30), while the mass flow of the HPC has a significant influence on the HP-System rotational speed N2 (0.64). N2 also reacts to the efficiency of the HPC/HPT (0.14/0.13). Furthermore, there is a significant relationship between N1 speed and the pressure ratio and the mass flow rate of the LPC (0.57/0.42). In addition, the pressure Pt5 reacts sensitively to efficiency of the LPC and LPT (0.23/0.24).

In order to illustrate the virtual process and to demonstrate the significance of the interactions on the overall performance, the described methods are performed with the real HPT blade in Figure 4 as an example. The geometry of the worn blade, roughness parameters, and of their confidence limits are derived and supplied to the process. Subsequently, the metamodel of the CFD is used to obtain the module aerodynamics and scaling factors. The HPT efficiency is reduced by 2.4 ± 0.2%, the pressure ratio is reduced by 0.046 ± 0.003, and the mass flow is increased by 0.64 ± 0.08 kg/s compared to new blades. These substantial aerodynamic changes of the scrapped HPT blade confirm the heavy deterioration stated earlier.

In the next step, these results are integrated in five aircraft engine configurations Θ by means of the performance metamodel. The configurations represent the following health conditions

1. Θ_1- deteriorated HPT
2. Θ_2- deteriorated HPT and LPC
3. Θ_3- deteriorated HPT, LPC, and IPC
4. Θ_4- deteriorated HPT, LPC, IPC, and HPC
5. Θ_5- deteriorated HPT, LPC, IPC, HPC, and LPT.

The scaling factors of the compressors and the LPT are based on the values in the Table 3. Besides, the influence of the HPT blade on the Tt5 is shown in Figure 11.

For this purpose, the Tt5 difference between the real and the new turbine blade over the various configurations Θ is shown. The red bar represents the influence of the HPT, the blue bar the influence of all other deteriorated modules on the Tt5 temperature. As expected, Tt5 increases the most due to a deteriorated HPT and HPC. It is particularly noticeable that the impact of a the HPT blade on the Tt5 is not constant for each configuration. Especially, for the aircraft engines Θ_3 and Θ_4, the difference decreases from 50 K to 41 K. This effect can be explained by the interdependence of the various modules, e.g. the throttling of the various compressors due to degradation. It agrees with the high global sensitivity previously described and already shown in Figure 10. The strength of these interaction effects is indicated by the red bars in Figure 10. The interaction effects are particularly significant for modules whose isolated influence is low (see IPC and Θ_3). The relationship and level between HPT deterioration and Tt5 is comparable to studies on real aircraft engines (see Zaita et al. (1997)).
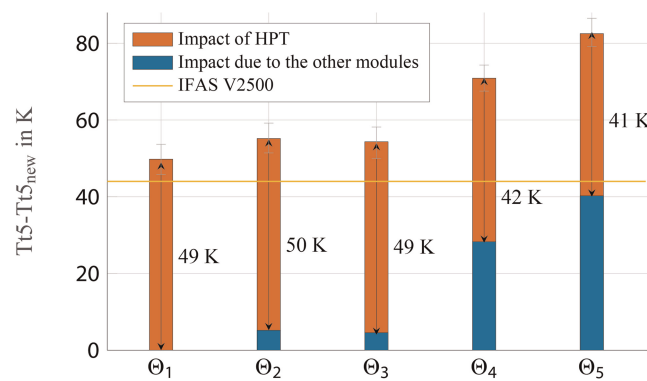
Figure 11. Impact on Tt5 of miscellaneous aircraft engine health conditions Θ using the example of the real HPT blade in Figure 4.

Conclusions

Variability in the modules due to production tolerances and wear directly affect the aircraft engine performance. To analyse this influence, a virtual process is developed which is able to predict overall aircraft engine performance, using the example of the first blade of the HPT in the V2500 turbofan engine. For this purpose, 36 deteriorated HPT blades are automatically digitised, their geometry evaluated, and their aero-thermodynamic effects determined at the level of the module. In a Gas Path Analysis of the HPT and the remaining modules (compressors and LPT), the overall aircraft engine performance is estimated. The use of CFD simulations for the HPT allows the local deterioration to be directly related to the engine performance, whereby a detailed understanding is established.

Based on the results of the physical models, metamodels are developed which are used to evaluate the isolated sensitivities within the HPT and isolated and interacting sensitivities within the aircraft engine. The results of variance-based sensitivity analysis can be summarised as:

1. Stagger angle γ of the HPT blade of the first stage has the most significant influence on η, π and $\dot{m}$ (see Figure 9).
2. Next to γ a relationship between tip gap and efficiency is detected; the remaining geometric variations only have a minor influence.
3. Tt5 and SFC react most strongly to η_{HPC} and η_{HPT}, Tt3 to $\dot{m}_{HPC}$ and $\dot{m}_{HPT}$, as well as N2 to $\dot{m}_{HPC}$, and N1 to $\dot{m}_{LPC}$ and π_{LPC} (see Figure 10).
4. The sensitivity of a module with geometric variances on the aircraft engine performance depends on the condition of the remaining modules (see Figure 11).

These results of this knowledge-based approach are used to improve detection and the understanding of the sensitivities of the overall engine performance to the blades' geometries, which is an essential area in production, as well as in maintenance, repair, and overhaul (MRO) and in operation. While studies of isolated modules might help to quantify the impact of geometric variations as a first step, the analysis of the whole aircraft engine is required to obtain accurate descriptions of the aircraft engine's efficiency and condition.

The virtual process described shows that virtual twins are capable of evaluating aircraft engine performance. It is possible to integrate such a performance assessment with the virtual twin of an MRO shop as a basis for a rule-based decision making on component regeneration. The virtual twin even shows the possibility of matching certain deteriorated modules with each other and how this will impact the overall aircraft engine.

In future studies, the HPT process shown can be directly applied for further module evaluations (e.g. HPC, LPC, and LPT) that can be implemented in the aircraft engine performance analysis to characterise additional local deterioration effects. Furthermore, the described simplifications can be addressed and eliminated by larger sample sizes for further increasing the process accuracy. Finally, it is possible to further increase the accuracy of the process using more samples to compensate for the simplifications described.

Nomenclature

$\dot{m}$	Mass Flow
η	Efficiency
γ	Stagger Angle

ω	Specific Dissipation Rate
π	Pressure Ratio
Θ	Jet Engine Configuration
AI	Artificial Intelligence
BPR	Bypass Ratio
C	Compressor
CAD	Computer-Aided Design
CFD	Computational Fluid Dynamics
DoE	Design of Experiment
E_P, E_P, E_N	Error Function
EASI	Effective Algorithm for Computing Global Sensitivity Indices
EGT, Tt5	Exhaust Gas Temperature
f	Model Function
F_N	Thrust
GL	Auxiliary Coordinates
H	Hidden Layer
h	Enthalpy
hp	High-Pressure
HPC	High-pressure Compressor
HPT	High-pressure Turbine
IAE	International Aero Engines
IPC	Intermediate-pressure Compressor (Booster)
k	Turbulent Kinetic Energy
k_s	Equivalent Sand-Grain Roughness
l	Airfoil Chord
l_p	Low-Pressure
LPC	Low-pressure Compressor (Fan)
LPT	Low-pressure Turbine
MRO	Maintenance, Repair and Overhaul
$N1$	Rotational Speed of LP-System
$N2$	Rotational Speed of HP-System
NLGPA	Non-linear Gas Path Analyse
$p(\cdot)$	Distribution Function
$p(\cdot, \cdot \mid \cdot)$	Conditional Probability Density Function
$p(\cdot, \cdot)$	Non-Conditional Probability Density Function
P	Pressure or Power
r	Tip Gap
r_{LE}	Leading Edge Radius
R_{SS}, R_{PS}	Roughness Suction/Pressure Side
S_a	Surface Parameter
S_y	First-Order Effect Kucherenko/Sobol Index
S_y^T	Total-Order Effect Kucherenko/Sobol Index
SF	Scaling Factor
SFC	Specific Fuel Composition
T	Turbine or Temperature
t	Total
t_{TE}	Trailing Edge Thickness
V	Variance
x_i	Real-Valued Random Input Variable
Y	Model
y^+	Non-dimensional Wall Distance

Acknowledgments

Competing interests

Jan Goeing declares that he has no conflict of interest. Hendrik Seehausen declares that he has no conflict of interest. Lennart Stania declares that he has no conflict of interest. Nicolas Nuebel declares that he has no conflict of interest. Julian Salomon declares that he has no conflict of interest. Panagiotis Ignatidis declares that he has no conflict of interest. Friedrich Dinkelacker declares that he has no conflict of interest. Michael Beet declares that he has no conflict of interest. Berend Denkena declares that he has no conflict of interest. Joerg R. Seume declares that he has no conflict of interest. Jens Friedrichs declares that he has no conflict of interest.

References

Aschenbruck J., Adamczuk R., and Seume J. R. (2014). Recent progress in turbine blade and compressor blisk regeneration. *Procedia CIRP* 22: 256–262.

Aurenhammer F. (1991). Voronoi diagrams—a survey of a fundamental geometric data structure. *ACM Computing Surveys (CSUR)*. 23 (3): 345–405. https://doi.org/10.1145/116873.116880

Bammert K. and Sandstede H. (1976). Influences of manufacturing tolerances and surface roughness of blades on the performance of turbines.

Ben Abdessalem A. and El-Hami A. (2014). Global sensitivity analysis and multi-objective optimisation of loading path in tube hydroforming process based on metamodelling techniques. *The International Journal of Advanced Manufacturing Technology*. 71 (5): 753–773. https://doi.org/10.1007/s00170-013-5518-4

Betker T., Quentin L., Kästner M., and Reithmeier E. (2020). 3d registration of multiple surface measurements using projected random patterns.

Bons J. (2005). A critical assessment of reynolds analogy for turbine flows. *Journal of Heat Transfer*. 127 (5): 472–485. https://doi.org/10.1115/1.1861919

Bons J. P. (2010). A review of surface roughness effects in gas turbines. *Journal of Turbomachinery*. 132: 021004. https://doi.org/10.1115/1.3066315

Cruz-Manzo S., Panov V., and Zhang Y. (2018). Gas path fault and degradation modelling in twin-shaft gas turbines. *Machines*. 6 (4): 43. https://doi.org/10.3390/machines6040043

Ernst B., Seume J. R., and Herbst F. (2016). Probabilistic cfd-analysis of regeneration-induced geometry variances in a low-pressure turbine. In 52nd AIAA/SAE/ASEE Joint Propulsion Conference, p. 4555.

Fentaye A. D., Baheta A. T., Gilani S. I., and Kyprianidis K. G. (2019). A review on gas turbine gas-path diagnostics: state-of-the-art methods, challenges and opportunities. *Aerospace*. 6 (7): 83. https://doi.org/10.3390/aerospace6070083

Franke M., Kuegeler E., and Nuernberger D. (2005). Das dlr-verfahren trace: Moderne simulationstechniken fuer turbomaschinenstroemungen. In DGLR Congress.

Gilge P., Kellersmann A., Friedrichs J., and Seume J. R. (2019). Surface roughness of real operationally used compressor blade and blisk. *Proceedings of the Institution of Mechanical Engineers, Part G: Journal of Aerospace Engineering*. 233 (14): 5321–5330.

Glen G. and Isaacs K. (2012). Estimating sobol sensitivity indices using correlations. *Environmental Modelling & Software*. 37: 157–166. https://doi.org/10.1016/j.envsoft.2012.03.014

Goeing J., Bode C., Friedrichs J., Seehausen H., Herbst F., and Seume J. R. (2020a). Performance simulation of roughness induced module variations of a jet propulsion by using pseudo bond graph theory. In Turbo Expo: Power for Land, Sea, and Air, Vol. 84058. American Society of Mechanical Engineers, p. V001T01A014.

Goeing J., Seehausen H., Pak V., Lueck S., Seume J. R., and Friedrichs J. (2020b). Influence of combined compressor and turbine deterioration on the overall performance of a jet engine using rans simulation and pseudo bond graph approach. *Journal of the Global Power and Propulsion Society*. 4: 296–308. https://doi.org/10.33737/jgpps/131109

Heinze K., Meyer M., Scharfenstein J., Voigt M., and Vogeler K. (2014). A parametric model for probabilistic analysis of turbine blades considering real geometric effects. *CEAS Aeronautical Journal*. 5 (1): 41–51. https://doi.org/10.1007/s13272-013-0088-6

Högner L., Nasuf A., Voigt P., Voigt M., Vogeler K., et al. (2016). Analysis of high pressure turbine nozzle guide vanes considering geometric variations. In Turbo Expo: Power for Land, Sea, and Air, Vol. 49712. American Society of Mechanical Engineers, p. V02CT45A025.

Hohenstein S., Aschenbruck J., and Seume J. (2013). Aerodynamic effects of non-uniform surface roughness on a turbine blade, Vol. 6A. In Turbomachinery of Turbo Expo: Power for Land, Sea, and Air.

Kato M. and Launder B. (1993). The modelling of turbulent flow around stationary and vibrating square cylinders. In Proceedings 9th Symposium on Turbulent Shear Flow, Kyoto, Japan, pp. 10.4.1–10.4.6.

Khan S. and Yairi T. (2018). A review on the application of deep learning in system health management. *Mechanical Systems and Signal Processing*. 107: 241–265. https://doi.org/10.1016/j.ymssp.2017.11.024

Kucherenko S., Tarantola S., and Annoni P. (2012). Estimation of global sensitivity indices for models with dependent variables. *Computer Physics Communications*. 183 (4): 937–946. https://doi.org/10.1016/j.cpc.2011.12.020

Kugeler E., Nurnberger D., Weber A., and Engel K. (2008). Influence of blade fillets on the performance of a 15 stage gas turbine compressor. In ASME Turbo Expo 2008: Power for Land, Sea, and Air, American Society of Mechanical Engineers, pp. 415–424.

Kurzke J. and Halliwell I. (2018). Propulsion and Power: An Exploration of Gas Turbine Performance Modeling. Cham, Switzerland: Springer.

Lavainne J. (2003). Sensitivity of a compressor repeating-stage to geometry variation. PhD thesis, Massachusetts Institute of Technology.

Maiwada B., Muaz N. I., Ibrahim S., and Musa S. M. (2016). Impacts of compressor fouling on the performance of gas turbine. *International Journal of Engineering Science and Computing*. 6 (3): 2118–2125.

McKay M. D., Beckman R. J., and Conover W. J. (2000). A comparison of three methods for selecting values of input variables in the analysis of output from a computer code. *Technometrics*. 42 (1): 55–61. https://doi.org/10.1080/00401706.2000.10485979

Merkl E. (2016). Uhbr aero engines, technologien für die nächste triebwerksgeneration (enoval). Deutsche Gesellschaft für Luft-und Raumfahrt-Lilienthal-Oberth eV. https://www.dglr.de/publikationen/2016/420025.pdf

Moré J. J. (1978). The levenberg-marquardt algorithm: implementation and theory. In: Numerical Analysis: Proceedings of the Biennial Conference Held at Dundee, June 28–July 1, 1977. Berlin, Heidelberg: Springer. pp. 105–116.

Nikuradse J. (1933). Law of flows in rough pipes, *NACA Technical Memorandum 1292*.

Nübel N. and Denkena B. (2022). *Digitaler Zwilling zur hochautomatisierten Einzelteilfertigung in der Reparatur*, TEWISS Verlag. ISBN 3959007140.

Nuernberger D. (2004). Implizite Zeitintegration fuer die Simulation von Turbomaschinenstroemungen. PhD thesis, Ruhr-Universitaet Bochum.

Plischke E. (2010). An effective algorithm for computing global sensitivity indices (easi). *Reliability Engineering & System Safety*. 95 (4): 354–360. https://doi.org/10.1016/j.ress.2009.11.005

Plischke E., Borgonovo E., and Smith C. L. (2013). Global sensitivity measures from given data. *European Journal of Operational Research*. 226 (3): 536–550. https://doi.org/10.1016/j.ejor.2012.11.047

Rafiq M., Bugmann G., and Easterbrook D. (2001). Neural network design for engineering applications. *Computers & Structures*. 79 (17): 1541–1552. https://doi.org/10.1016/S0045-7949(01)00039-6

Reitz G., Kellersmann A., Schlange S., and Friedrichs J. (2018). Comparison of sensitivities to geometrical properties of front and aft high pressure compressor stages. *CEAS Aeronautical Journal*. 9 (1): 135–146. https://doi.org/10.1007/s13272-018-0281-8

Salomon J., Göing J., Lück S., Broggi M., Friedrichs J., and Beer M. (2021). Sensitivity analysis of an aircraft engine model under consideration of dependent variables. In Turbo Expo: Power for Land, Sea, and Air, Vol. 84898. American Society of Mechanical Engineers, p. V001T01A005.

Saltelli A., Tarantola S., Campolongo F., and Ratto M. (2004). Sensitivity Analysis in Practice: A Guide to Assessing Scientific Models, Vol. 1. New York: Wiley.

Saltelli A., Annoni P., Azzini I., Campolongo F., Ratto M., and Tarantola S. (2010). Variance based sensitivity analysis of model output. design and estimator for the total sensitivity index. *Computer Physics Communications*. 181 (2): 259–270. https://doi.org/10.1016/j.cpc.2009.09.018

Samarasinghe S. (2006). Neural networks for applied sciences and engineering: from fundamentals to complex pattern recognition, 1st edition. New York: Auerbach Publications.

Scharfenstein J., Heinze K., Voigt M., Vogeler K., and Meyer M. (2013). Probabilistic cfd analysis of high pressure turbine blades considering real geometric effects. In Turbo Expo: Power for Land, Sea, and Air, Vol. 55232. American Society of Mechanical Engineers, p. V06BT43A005.

Schlichting H. (1936). Experimentelle untersuchungen zum rauhigkeitsproblem. *Archive of Applied Mechanics*. 7 (1): 1–34.

Schwerdt L., Hauptmann T., Kunin A., Seume J. R., Wallaschek J., et al. (2017). Aerodynamical and structural analysis of operationally used turbine blades. *Procedia CIRP*. 59: 77–82. https://doi.org/10.1016/j.procir.2016.09.023

Seehausen H., Gilge P., Kellersmann A., Friedrichs J., and Herbst F. (2020). Numerical study of stage roughness variations in a high pressure compressor. *International Journal of Gas Turbine, Propulsion and Power Systems*. 11 (3): 16–25. https://doi.org/10.38036/jgpp.11.3_16

Shahsavani D. and Grimvall A. (2011). Variance-based sensitivity analysis of model outputs using surrogate models. *Environmental Modelling & Software*. 26 (6): 723–730. https://doi.org/10.1016/j.envsoft.2011.01.002

Sigal A. and Danberg J. E. (1990). New correlation of roughness density effect on the turbulent boundary layer. *AIAA Journal*. 28 (3): 554–556. https://doi.org/10.2514/3.10427

Sobol I. M. (2001). Global sensitivity indices for nonlinear mathematical models and their monte carlo estimates. *Mathematics and Computers in Simulation*. 55 (1–3): 271–280. https://doi.org/10.1016/S0378-4754(00)00270-6

Spieler S., Staudacher S., Fiola R., Sahm P., and Weißschuh M. (2008). Probabilistic engine performance scatter and deterioration modeling. *Journal of Engineering for Gas Turbines and Power*. 130 (4): 042507-1–042507-9. https://doi.org/10.1115/1.2800351

Volponi A. J. (2014). Gas turbine engine health management: past, present, and future trends. *Journal of Engineering for Gas Turbines and Power*. 136 (5): 051201-1–051201-20. https://doi.org/10.1115/1.4026126

von der Bank R., Donnerhack S., Rae A., Cazalens M., Lundbladh A., and Dietz M. (2014). Lemcotec: Improving the core-engine thermal efficiency. In Turbo Expo: Power for Land, Sea, and Air, Vol. 45578. American Society of Mechanical Engineers, p. V01AT01A001.

Wilcox D. C. (1988). Reassessment of the scale-determining equation for advanced turbulence models. *AIAA Journal*. 26 (11): 1299–1310. https://doi.org/10.2514/3.10041

Yaras M. and Sjolander S. (1992). Prediction of tip-leakage losses in axial turbines.

Zaita A. V., Buley G., and Karlsons G. (1997). Performance deterioration modeling in aircraft gas turbine engines. In Turbo Expo: Power for Land, Sea, and Air, Vol. 78712. American Society of Mechanical Engineers, p. V004T16A007.